IEEE Access
Multidisciplinary | Rapid Review | Open Access Journal

Date of publication xxxx 00, 0000, date of current version xxxx 00, 0000.

Digital Object Identifier 10.1109/ACCESS.2017.Doi Number

A review of the space environment effects on spacecraft in different orbits

Yifan Lu[1*], Qi Shao[1], Honghao Yue[1], Fei Yang[1]

[1] State Key Laboratory of Robotics and System, Harbin Institute of Technology, Harbin 150001, China

Corresponding author: Yifan Lu (e-mail: yf.lu@hit.edu.cn).

This research was supported by the National Natural Science Foundation of China (Grant No. 51835002) and Self-Planned Task of State Key Laboratory of Robotics and System (HIT) (Grant No. SKLRS201808B).

ABSTRACT The space environment consists of various complex phenomena, which could have a strong influence on the spacecraft operation in different aspects. Since the very beginning of the space exploration, numerous studies have been done on space environment. However, most of the existing literatures focus on the investigation of the details of environmental phenomena, while the space environment has rarely been discussed from the perspective of orbits types. Therefore, a comprehensive review on analyzing and comparing the environmental characteristics among diverse orbits in space is of great significance. In this paper, the main components of the space environment are introduced, including the neutral atmosphere, the plasma environment, the radiation environment, the macroscopic particle environment, the geomagnetic field, the temperature field, and the solar activities, etc. The relations of the various space environmental components are also discussed. The dominant environmental components and their effects on spacecraft in different orbits, i.e., the geosynchronous orbit (GEO), the low earth orbit (LEO), the medium earth orbit (MEO), and the high earth orbit (HEO), are investigated respectively. The space environment that should be taken into particular consideration is summed up to facilitate the design of the spacecraft in a specific orbit.

INDEX TERMS Space environment, spacecraft design, geosynchronous orbit, low earth orbit, medium earth orbit, high earth orbit

I. INTRODUCTION

More and more spacecraft are placed at different altitudes due to the momentous strategic position of space exploration. Generally speaking, the earth's space is divided into three regions. LEO is defined as the region from 160 km to 2000 km [1], which is the main affected zone of the upper atmosphere. MEO and HEO are separated by GEO which is at an altitude of 35786 km [2]. Table 1 shows the number of operating satellites in four types of orbits respectively according to the database producing by the Union of Concerned Scientists (UCS) [3]. It can be learnt that over half of the satellites are placed in LEO, and others are densely arranged in the vicinity of GEO. While MEO and the highly elliptical orbit have a few satellites by contrast.

Various spacecraft is distributed in a wide range of types of orbits, as shown in Figure 1. In MEO and HEO (M&H), various satellites are arranged near the semi-geosynchronous orbit and GEO. While there are more abundant spacecraft in LEO, including the International Space Station, the Hubble space telescope, and the manned spacecraft. However, countless anomalies resulted from various harsh space environment are taken place in different orbits all the time [4-5]. To ensure the reliability of spacecraft operation in the long term, particular emphasis should be put on eliminating the main impacts of the space environment on the spacecraft in different orbits.

TABLE I
THE NUMBER OF SATELLITES IN DIFFERENT ORBITS (INCLUDES LAUNCHES THROUGH 11/30/18).

The earth orbit	Number
LEO	1232
MEO	126
GEO	558
The highly elliptical orbit	41

This article has been accepted for publication in a future issue of this journal, but has not been fully edited. Content may change prior to final publication. Citation information: DOI 10.1109/ACCESS.2019.2927811, IEEE Access

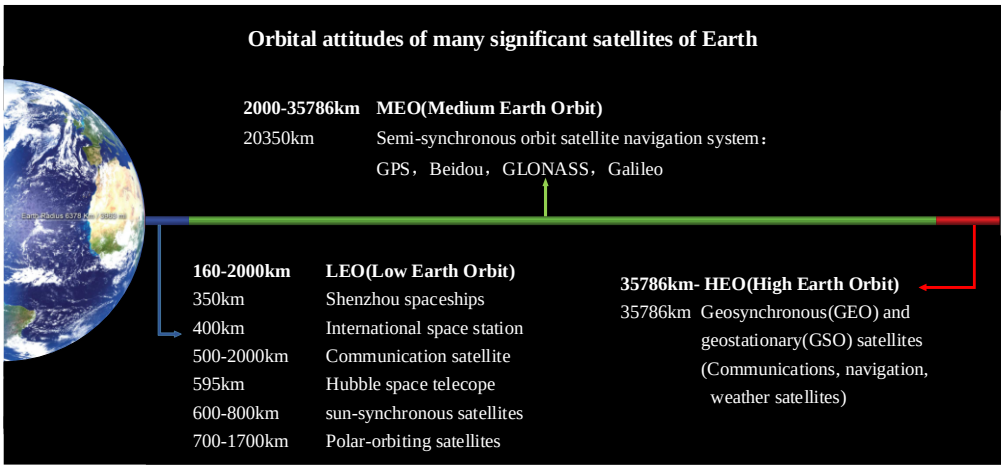

FIGURE 1. The distribution of important spacecraft in earth orbits.

In this paper, a review of the space environment and its effects on spacecraft in different orbits are given. In Section 2, the main space environment components are briefly investigated, including the neutral atmosphere, the plasma, the radiation, the macroscopic particles, the geomagnetic field, the temperature field, and solar activities. The geomagnetic field and solar activities are only discussed in Section 2, because they are usually apt to influence other environment components other than directly affect the spacecraft. In Section 3 and Section 4, the typical space environment components of LEO and M&H are classified. Specifically, the characteristics, effects on spacecraft, analyzing models, and preventing measures of these components are introduced, respectively. The unique properties of the two regions are presented by comparing the different behaviors of the same environment components.

The purpose of this paper is to provide a description of the space environment effects that need to be concerned in different orbits, and to serve as guidance for spacecraft maintenance. What should be noted is that the orbit-attitude perturbation analysis is not within the scope of this paper.

II. THE SPACE ENVIRONMENT COMPONENTS

NASA Marshall Space Flight Center describes the space environment as seven areas: the neutral atmosphere, the plasma, the radiation, meteoroids/orbital debris, thermal environment, and solar environment [6]. Since the effects of the solar environment are mainly to disturb other components, the space environment related to spacecraft operation is categorized into six areas, including the neutral atmosphere, the plasma, the radiation, the macroscopic particles [7], the geomagnetic field, and the temperature field. Different as causes and effects are, assorted environment components are intrinsically connected. When stimulated by external disturbance, a series of disturbing reactions would arise in the space.

A. THE NEUTRAL ATMOSPHERE

The neutral atmosphere includes the upper atmosphere and the gas releasing from the spacecraft surface, and the former accounts for the main part. The effects of the neutral atmosphere consist of the atmospheric drag and the atomic oxygen effects.

As the main perturbative force in LEO, atmospheric drag has a vital influence on the shape and altitude of orbits. Nevertheless, since the orbit-attitude perturbation analysis is not the content of this paper, atmospheric drag will not be discussed in more details.

Atomic oxygen is produced by the decomposition of the neutral atmosphere under the cosmic rays. As the dominant atmosphere component in the area ranging from 200 km to 800 km, atomic oxygen accounts for 80% of the total composition in the upper atmosphere [8]. The flux of atomic oxygen is influenced by the altitude and inclination of orbits, solar cycle, geomagnetic disturbance, and seasonal cycle. Although atomic oxygen in space is far from dense, the average impact energy collided with spacecraft operating at a speed of 7-8 km/s can up to 4-5 eV [9], which is sufficient for breaking the chemical bonds of many materials. Additionally, atomic oxygen erodes the surface of materials due to its strong oxidizability. Figure 2 shows the photographs of MISSE 2 PEACE polymers before and after the exposure to atomic oxygen [10]. Moreover, the eroded organic materials would generate condensable gas volatiles, which can lead to performance degradation and contamination of optical instruments [10-12].

Additionally, vacuum is another main phenomenon of the space environment, and the earth's space is chiefly under ultra-high vacuum. In this condition, there would be adverse effects on spacecraft, such as pressure difference, discharging, out-gassing, adhesion and cold welding, materials evaporation, sublimation, and decomposition. Not only would these effects disturb other phenomena, but also bring about the loss of mass and performance, molecular pollution, and damage of instruments, etc.

This article has been accepted for publication in a future issue of this journal, but has not been fully edited. Content may change prior to final publication. Citation information: DOI 10.1109/ACCESS.2019.2927811, IEEE Access

FIGURE 2. Pre-flight and post-flight photograph of the MISSE 2 PEACE polymers experiment tray [10].

B. THE PLASMA ENVIRONMENT

The plasma is quasi-neutral to the outside, and primarily composited by electrons and ions, accounting for almost 99% in cosmic substances [13]. The manifold plasma environment in the earth's space is made up of the ionospheric plasma, magnetospheric plasma, and solar wind plasma, which are created by the interactions among solar radiation, geomagnetic field, and the upper atmosphere. The plasma in space can be classified into hot plasma and cold plasma. Even if both of them engender surface charging, hot plasma is more threatening. The plasma generated in the earth space is mostly cold plasma, whose density and energy spectrum differ with altitude. When bombarded by the solar wind, some of the cold plasma has great chances to turn into hot plasma.

Surface charging can bring about electrostatic discharge, electromagnetic pulse jamming, solar array power loss and short circuit, material performance degradation, and accelerating contamination [14]. Figure 3 displays the burnt damage of the solar array owing to secondary discharge. On the other side, some researchers have come up with the concept that the spacecraft is defended against low-orbit spy satellites by utilizing the disturbance and destruction resulted in plasma [15]. Plentiful theoretical models are established regarding surface charging, based on satellites measurement and ground simulation [16]. The simulation for surface charging in different orbits is realized by bountiful algorithms [17-19]. Currently, the most versatile simulation software are NASCAP, SPIS, MUSCAT [20]. In addition to passive measures such as limiting resistivity, earthing, and electromagnetic shielding, active control of potential is also an effective way to accomplish the prevention of surface charging [21-22].

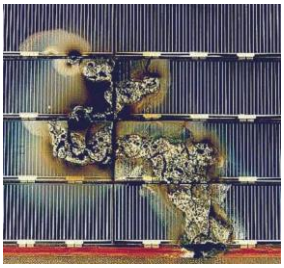

FIGURE 3. The damage of solar array caused by arcing in ESA EURECA [14].

C. THE RADIATION ENVIRONMENT

Statistically, the anomalies caused by radiation account for approximately 40% of the total problems induced by the space environment [23]. The high-energy particles generating radiation are mainly protons, electrons, and heavy ions, which are originated from sediment in high latitude, Van Allen radiation belt, the solar cosmic ray, and the galactic cosmic ray. Since the influence of the galactic cosmic ray is much less than Van Allen radiation belt and the solar cosmic ray, it would not be taken into consideration in this paper.

Unlike the surface charging caused by plasma, high-energy particles can penetrate the surface of spacecraft, resulting in the displacement damage, internal charging, and single event effects [24]. What is more, A long-term Exposure in high-energy particles environment can lead to radiation dose damage [25]. These effects mentioned above tends to create detriments to sensitive apparatus and data processing, etc., because of problems like logic circuits flipping [26]. Figure 4 displays the disservice to sensors, charge-coupled devices (CCD), and field-effect tubes (FET) caused by radiation.

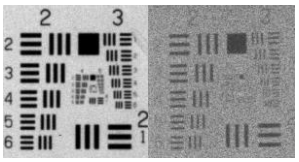

(a) Original frames obtained by sensors with a radiation dose of 3kGy and 10kGy.

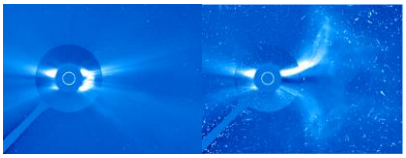

(b) CCD photographs from SOHO before and after displacement damage.

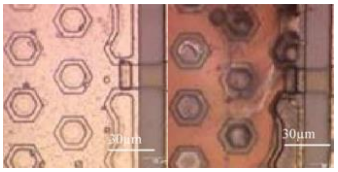

(c) Photographs of FET before and after the burnt caused by the single-event effect.

FIGURE 4. The impacts of high-energy particles [24, 26].

Since high-energy protons are the main cause of displacement damage and single-event effect, it is crucial to anticipate their distribution and flux by modeling and simulating. Models for high-energy protons coming from Van Allen radiation belt and solar activities are established respectively, such as AP-8 and ESP [27-28]. And models for high-energy electrons are established as well, such as AE-8 and FLUMIC [29-30]. They realize prediction with the help of corresponding software [31-33]. It is noted that models are required to be selected according to their applicable conditions. The spacecraft could be protected by passive measures, including satellites orbit transferring and radiation

This article has been accepted for publication in a future issue of this journal, but has not been fully edited. Content may change prior to final publication. Citation information: DOI 10.1109/ACCESS.2019.2927811, IEEE Access

hardening technologies, and active techniques taking advantages of low-frequency radio waves, magnetic fields, and electric fields [34-37].

The earth's radiation belt, also known as the Van Allen radiation belt, gathers high-energy particles captured and bonded by the geomagnetic field. It consists of the inner radiation belt and the outer radiation belt, as shown in Figure 5. The inner radiation belt is the region ranging from 600 km to 10000 km, where high-energy protons predominate. Shielded by the geomagnetic field, the inner belt is barely affected by solar activities and therefore keeps stable. However, the intensity of the inner belt in low altitude lessens sharply as the altitude decreases due to the collision between particles and upper atmosphere molecules. The outer radiation belt is the region ranging from 13000 km to 45000 km, where high-energy electrons predominate. Owing to the weak protection by the geomagnetic field near the magnetopause, the high-energy electrons are susceptible to solar activities, repeating the decay-growth cycling [38-40].

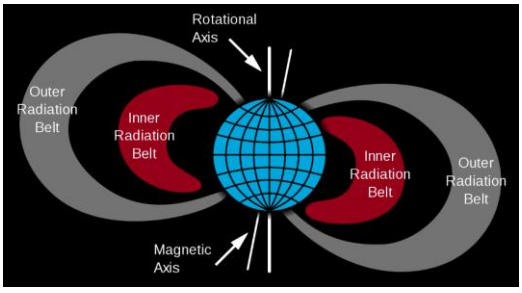

FIGURE 5. **The structure of the Van Allen radiation belt [41].**

The solar cosmic ray is the stream of high-energy particles generated by solar activities, with high intensity in a short duration. In the period of the solar flare, numerous high-energy particles, most of which are protons. And this is what we called the solar proton event. This makes the radiation environment worse, especially in M&H and polar orbits.

D. MACROSCOPIC PARTICLE ENVIRONMENT

The macroscopic particles refer to space debris and micrometeoroids. Space debris is derived from human space activities, while micrometeoroids are evolved from asteroids and comets. The impacts of both of them can bring about damage, as shown in Figure 6.

According to the size and the hazard, space debris can be categorized into three classes. Fragments larger than 10 cm in diameter are called large-sized debris, while those smaller than 1 cm in diameter are called small-sized debris. And fragments whose size are between the first two types are called medium-sized debris [42]. Though the large-sized debris can bring devastating destruction to the spacecraft, it has a low flux. Whereupon circumvention of large-sized debris should be carried out pursuant to ground-based monitoring. Not only does the small-sized debris have a high flux, but also it can bring physical damage to the spacecraft, such as performance degradation of optical devices [43]. Besides, secondary destructions of internal structures and the plasma cloud forming by ultra-high-speed impacting would make the situation more troublesome. Whereupon forecasting and preventing measures are supposed to be implemented to small-sized debris pursuant to space-based monitoring [44-45]. The medium-sized debris is difficult to be observed and therefore hard to be avoided [46]. And that is why it is classified as dangerous debris even if it has a lower flux than that of the small-sized debris. Encountering with micrometeoroids is random, and their trajectory is arduous to be detected from ground-based radars. Since the millimeter-scale micrometeoroids threaten the operation of the spacecraft, preventing measures are obliged to be applied [47-49].

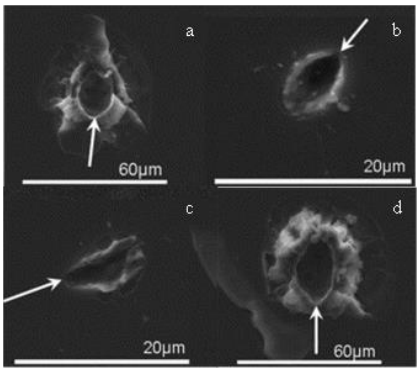

FIGURE 6. **The shape of small impact: (a) and (b) space debris impacts; (c) and (d) micrometeoroid impacts. The white arrows illustrate the likely impactor trajectory [43].**

Although space debris and micrometeoroids both would impact the spacecraft, they differ in physical properties and motion features. Space debris, with a density of 2.8 g/cm^3, often travels in a circular orbit. Space debris usually impacts spacecraft operating in the same orbit as it does. The impact velocity is related to the inclination of orbits as well as the orientation of the spacecraft surface, and the average impact velocity of space debris is about 10 km/s. In contrast, micrometeoroids, whose density is 0.5 g/cm^3, impact the spacecraft from all directions with an average impact velocity up to20 km/s [50-52].

The number of space debris and micrometeoroids varies with the altitude of orbits, as shown in Figure 7 and Figure 8. The object count of space debris in LEO has always been accounting for a high proportion. Besides, the object count in other commonly used orbits has also risen distinctively in recent years. The flux of micrometeoroids is indicated by a combined factor which takes the earth shielding effect and gravitational convergence effect into consideration [53]. It is palpable in Figure 8 that the flux upsoars as altitudes grow in LEO, reaching the peak in the altitude about 2500 km. Contrasted with part region of M&H, the LEO is much threatened with micrometeoroids.

This article has been accepted for publication in a future issue of this journal, but has not been fully edited. Content may change prior to final publication. Citation information: DOI 10.1109/ACCESS.2019.2927811, IEEE Access

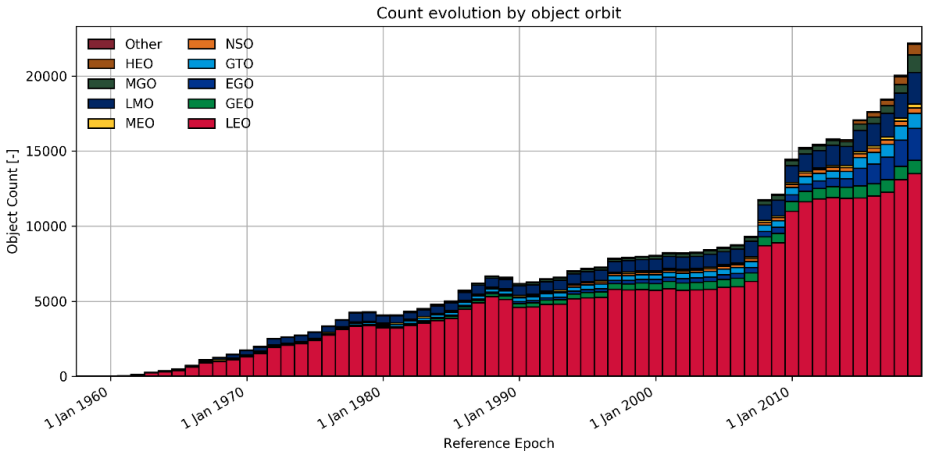

FIGURE 7. **Statistics and prediction of the number of space debris in common orbit by ESA [54].**

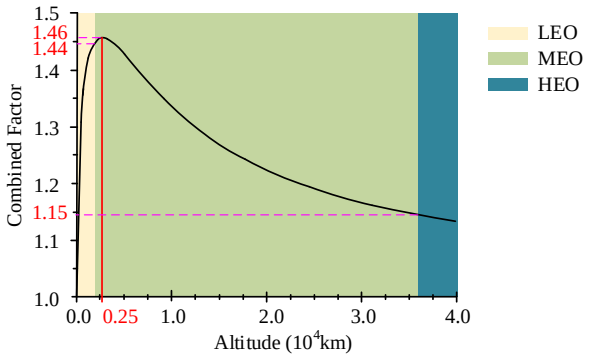

FIGURE 8. **The combined factor of micrometeoroids varies with altitudes [53].**

To keep the spacecraft out of the impact of macroscopic particles, the expert systems for forecasting and protecting need to be established, founded on observation, modeling and simulation. By now, there has been developed plenty of observing systems and sensing methods, such as SSN and TIRA [55]. In the meanwhile, radars based on ground and space as well as optical measurements have been employed [56]. They predict the trajectories and orbits of macroscopic particles with approaches varying with altitudes and sizes [57]. Mathematical models are established for debris models, such as CODR, IDES [58], and micrometeoroid models, such as Cours-Palais, Grün, Divine-Staubach [59-61], as well as collision models, such as Frye, Chobotov [62-63]. They are applied to evolution in different time span and engineering prediction for all kinds of particles. Whereupon warning procedures, such as BMBER, MDPANTO, etc., are developed, in terms of the flux, parameters, orbits, and time span of macroscopic particles [64-65]. They are able to assess the damage, detectivities, avoidance strategies, and effectiveness of mitigation measures. Based on the experiments and simulations of impacting in an ultra-high-speed [66-67], the protecting measures like shield structures prove to be adequate for millimeter scale macroscopic particles [68].

Due to the perturbation, the natural dying out of macroscopic particles basically depends on falling into the atmosphere and burning down. In consequence, the lifespan of space debris is in connection with the altitude of orbits. Space debris in LEO can exist around decades to a hundred years, while those in M&H could remain for hundreds or even thousands of years. As stated by statistics from ESA, by the end of January 2019, the mass of all space debris in the earth's space has exceeded 8000 tons, especially dangerous debris and large-sized debris, as shown in Table 2. Environmental management has to be carried out, otherwise, LEO would reach the state of super-critical, where the cascade collision among space objects would devastate orbit resources [69]. And therefore measures should be transferred to active removal from passive protection. At present, measures against dangerous macroscopic particles include energy dissipation, tethering, recovery, and deorbiting [70-72]. In various active removal techniques like capturing [73-75], removal by laser has an outstanding prospect of engineering application, space-based laser in particular [76-79], as sketched in Figure 9.

TABLE II
STATISTICS OF SPACE DEBRIS (UP TO JANUARY 2019) [80].

The size of space debris	Object count ($\times 10^4$)
>10cm	3.4
1cm~10cm	90
1mm~1cm	12800

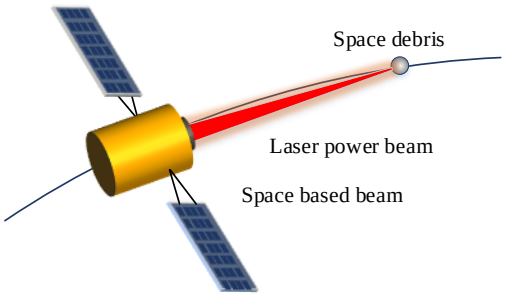

FIGURE 9. **Schematic diagram of space-based laser removal of space debris.**

This article has been accepted for publication in a future issue of this journal, but has not been fully edited. Content may change prior to final publication. Citation information: DOI 10.1109/ACCESS.2019.2927811, IEEE Access

E. THE GEOMAGNETIC FIELD

The geomagnetic field ranges from the earth's core to the magnetopause with low intensity. Since the intensity decreases outward at the speed of r^{-3}, the geomagnetic field is getting stronger as the altitude reduces. And thus LEO is the main region that the geomagnetic field has effects on [81]. Because the intensity varies with latitude in the same altitude, the geomagnetic field is relatively strong near the polar area [82]. The severe influence on the near-earth geomagnetic field comes from the solar wind, the high-speed plasma in which could induce global-scale geomagnetic storms. The geomagnetic storms would disturb the upper atmosphere and particle environment, leading to ionospheric storms and high-energy electron storms, and enhancing other adverse effects therewith [83]. Badly squeezed by the solar wind, the altitude of magnetopause diminishes from10 Re (Re is the radius of the earth) to 3-5 Re [84]. For this reason, spacecraft in HEO and part region of MEO stands great chances to lose the shielding of the geomagnetic field completely, exposed to the harsh radiation environment of the solar wind.

As a geomagnetic field model recommended by the International Geomagnetic and Upper Air Physics Society, the International Geomagnetic Reference Field (IGRF) is an international standard for studying the geomagnetic field [85]. According to models and formulae, the intensity of the geomagnetic field at a specific time and place could be available.

F. THE TEMPERATURE FIELD

The external thermal conditions of the spacecraft in space include the solar radiation, the earth infrared, and the earth albedo, which are collectively known as space external heat, as outlined in Figure 10. While the space is equivalent to the absolute black body compared with spacecraft, acting as a heat sink. In addition, the temperature field of spacecraft is related to waste heat and circulating heat generated by itself as well. However, since the internal temperature change has little to do with the external temperature of outer parts, it can be ignored when the temperature field of outer parts is studied. In the course of periodic motion, there is mutual occlusion occurring among the spacecraft, the Earth, and the Sun, as well as among different parts of the spacecraft. For this reason, space external heat experiences a cyclic variation. Besides, space external heat fluctuates periodically with the angle of radiation changing [86].

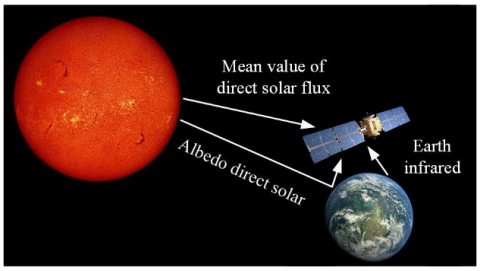

FIGURE 10. Schematic diagram of space external heat of the spacecraft.

The ultra-high vacuum determines that thermal radiation is the primary way of heat exchange between the space environment and the spacecraft, while the interior of the spacecraft could realize heat conduction. in addition, the analysis of the temperature field is supposed to be investigated whether the occlusion is taken into consideration in terms of the thermal conduction model and radiation model. The solar radiation is stable, which occupies the main proportion of external heat. However, the intensity of the earth infrared and albedo has much to do with factors including the atmosphere, surface temperature, and time. As a result, it is hard to quantify them accurately, and simplified models have come into common usage [87-88]. The mathematical expressions of the temperature field are established, considering the variation with orbits and operations. Whereupon, a series of procedures are developed, such as SINDA/G, I-DEAS TMG, etc. [89].

Among all the phenomena which are hostile to the spacecraft, the temperature-induced anomalies account for 11% [23]. Due to the alternate heating by space external heat and cooling by the cold black environment, the temperature of spacecraft changes dramatically, especially when entering and exiting the shadow region and the sunshiny region. As a consequence, the in-orbit spacecraft experiences large temperature difference and gradient, leading to thermal deformation and vibration, and bringing about anomalies like signal errors therewith. With the help of ground expeirments and simulations [90], thermal control measures ought to lay stress on preventing temperature soaring distinctively and stabilizing it. Passive measures must be taken including reasonable arrangement, adoption of appropriate materials and hardware, and rational organization of heat exchange [91]. Active measures should be applied as well, including adaptive adjustment of heat exchange parameters and temperature compensation [92-93]. However, since solar ultraviolet radiation can damage materials, thermal control facilities demand the anti-ultraviolet radiation ability [94].

G. SOLAR ACTIVITIES

The solar storm is a large-scale energy release occurring in the solar atmosphere for a short time. Energy is released in the forms of enhanced electromagnetic radiation, high-energy particles, and plasma cloud, as described in Figure 11.

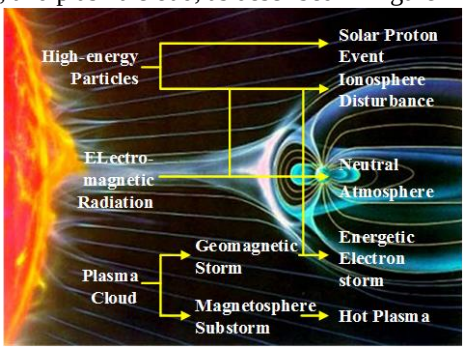

FIGURE 11. Schematic diagram of the effect of solar storms on the near-earth space environment.

This article has been accepted for publication in a future issue of this journal, but has not been fully edited. Content may change prior to final publication. Citation information: DOI 10.1109/ACCESS.2019.2927811, IEEE Access

The electromagnetic radiation (mainly X-ray) generated by solar storms propagates at the speed of light, taking merely 8 minutes to reach the earth and causing sudden ionospheric disturbances therewith. At that point, the amplitude and phase of the radio signal would change rapidly, leading to communication confusion between the satellite and ground. The high-energy particles spend at least dozens of minutes to reach the earth, acting directly on the spacecraft in M&H and polar orbits and causing serious radiation damage therewith. It costs the plasma cloud 1 to 3 days to reach the earth, inducing the global-scale geomagnetic storm. And therefore, it brings about various subsequent secondary disturbances, such as high-energy electrons storms, ionospheric storms, hot plasma injection, and the upper atmosphere densification [95]. In a nutshell, the substances and energy ejected from solar storms interact intricately with the earth's space environment, imperiling the operation of spacecraft.

H. SUMMARY

There are numerous components affecting the spacecraft, varying with altitude. In order to defend the spacecraft against those effects of phenomena efficiently, it is essential to summarize the characteristic of the space environment at a specific altitude, as outlined in Figure 12.

Except for the effects of vacuum, the gradation of colors indicates the severity of the space environment components. The vacuum effects exist continuously in the region higher than its minimum altitude. It is discernible from Figure 12 that the atomic oxygen effects and strong geomagnetic field are peculiar to LEO, while other components are altitude-varying. The ionospheric plasma and high-energy particles of the inner radiation belt maintain the upper hand in the particle environment in LEO, and the latter is primarily prevailing in the South Atlantic Anomaly and high latitude. In contrast, the particle environment in M&H consists of plasma, which comes from the geomagnetic field and solar wind, as well as high-energy particles, which come from Van Allen radiation belt and solar activities. On the other side, there are four density peaks of space debris and one flux peak of micrometeoroids in the space that spacecraft can operate. All in all, the macroscopic particle environment in LEO is much worse than that in M&H.

Figure 12 offers a quick idea about the phenomena by organizing those space environment components quantitatively by altitude. In this way, the types and severities of those components in a specific altitude are able to be consulted.

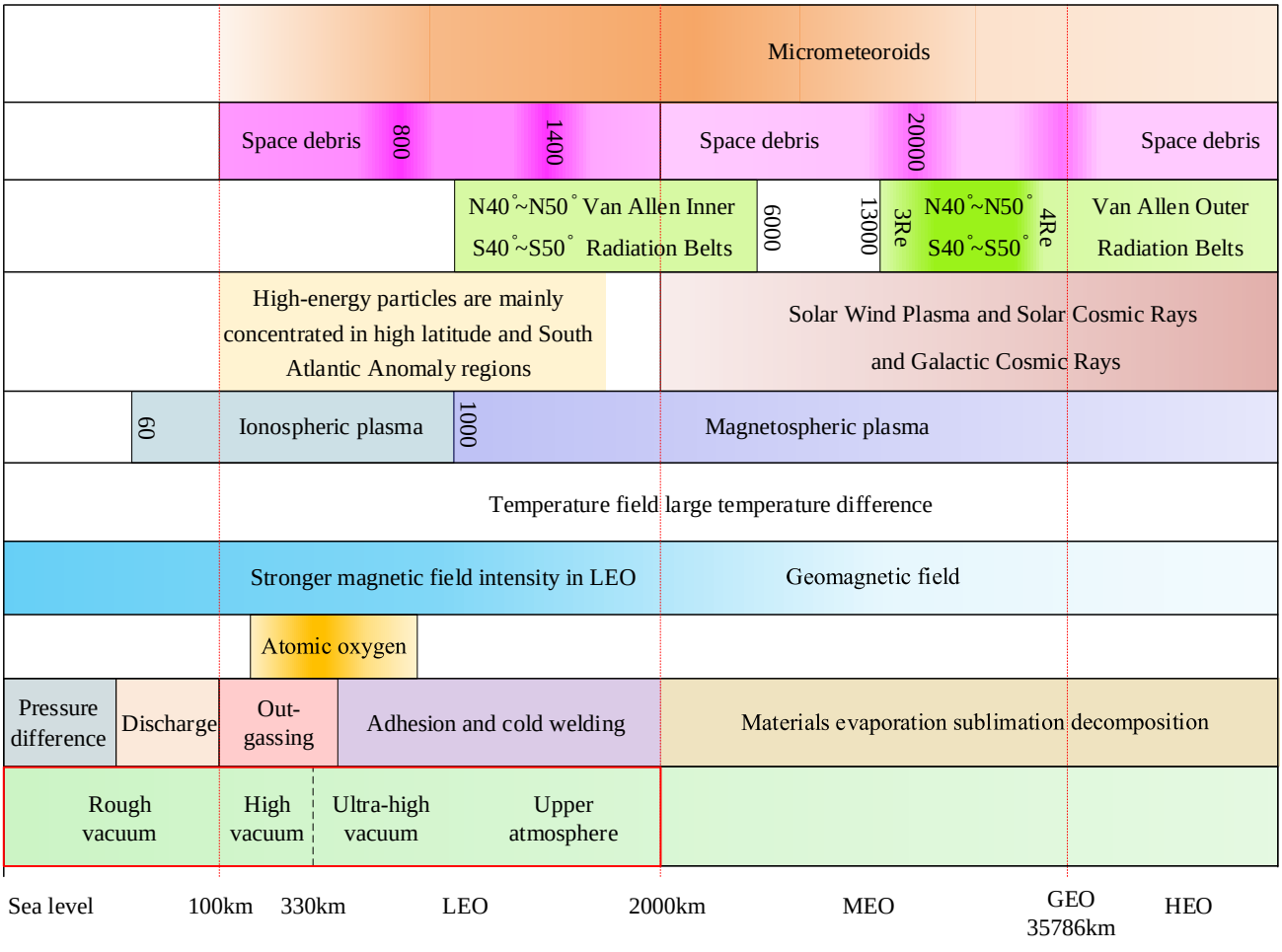

FIGURE 12. Space environmental components in all altitudes.

This article has been accepted for publication in a future issue of this journal, but has not been fully edited. Content may change prior to final publication. Citation information: DOI 10.1109/ACCESS.2019.2927811, IEEE Access

III. THE SPACE ENVIRONMENT IN LEO

LEO is a region ranging from 160 km to 2000 km. There are a series of satellites in this area, used for communication, detection [96], etc. Furthermore, LEO accommodates various common spacecraft, such as the manned spacecraft, Hubble Space Telescope, and the International Space Station. Nevertheless, the space environment in LEO is considerably complicated. The space environment of LEO contains the neutral atmosphere, ionospheric plasma, the inner radiation belt, macroscopic particle environment, and the temperature field. Additionally, the geomagnetic field and solar activities would disturb these phenomena to varying degrees.

A. THE ATOMIC OXYGEN

The neutral atmosphere is unique to LEO, in which atomic oxygen is the principal component that detriments the spacecraft. The atomic oxygen gains a great proportion in the upper atmosphere, and is affected by many factors, as mentioned in Section 2.1. For the reason that atomic oxygen puts the spacecraft in jeopardy of denudation, erosion, and oxidation [97], lots of researches have proposed diverse theoretical models about the atomic oxygen effects [98-100]. Moreover, with regard to preventing measures against atomic oxygen, the most studied aspects are anti-corrosive materials and coatings [101-102]. In the meanwhile, the results of ground experiments are not quite the same as the actual values [103]. And therefore numerical models [104-105] and simulation technologies [106-108] are developed to satisfy the demands of numerical verifications.

B. THE IONOSPHERIC PLASMA

The ionosphere is the region higher than 60 km, where plasma is cold and quasi-neutral with high density and low energy. The single Maxwell distribution function is able to describe the variation of the electron density with altitude and diurnal change (see Figure 13). The ionosphere is divided into four regions in altitude named as D, E, F1, F2 according to the electron density, in which F has the densest electrons [109]. The regions in low latitude have denser electrons and more violent anomalous changes than regions in high latitude. Since the variations are connected with the earth's activities, bountiful studies have been conducted on the relations between ionospheric precursors and earthquake [110-111].

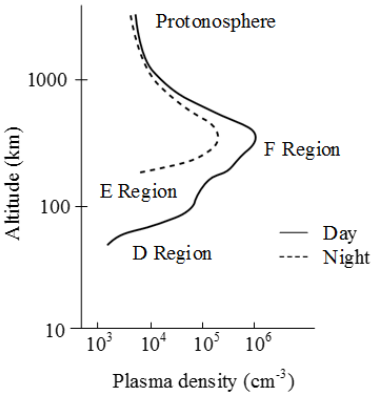

FIGURE 13. The structure of ionospheric plasma density [109].

The polar orbit is a special type of orbits in LEO, where hot plasma is sedimented in the background of dense cold plasma. As a result, the dual Maxwell function should be applied to the description of the plasma environment in polar orbits [112]. When geomagnetic field and solar activities disturb, the spacecraft passing through the polar area would be charged to negative hundreds of volts or even kilovolts.

The ionosphere is a lossy medium when transmitting radio waves. The dense electrons could enhance the attenuation of the signal [113]. Besides, the illumination of the sun has an influence on the ionosphere [114]. More severely, the solar activities could induce rapid and uneven fluctuations to the electron density, which in turn lead to the sudden ionosphere disturbances. At that time, the amplitude and phase of the radio signal which travels through the ionosphere would fluctuate fast, affecting the propagation of signals in all frequency bands, as shown in Figure 14. The severest case is communication interruption [115].

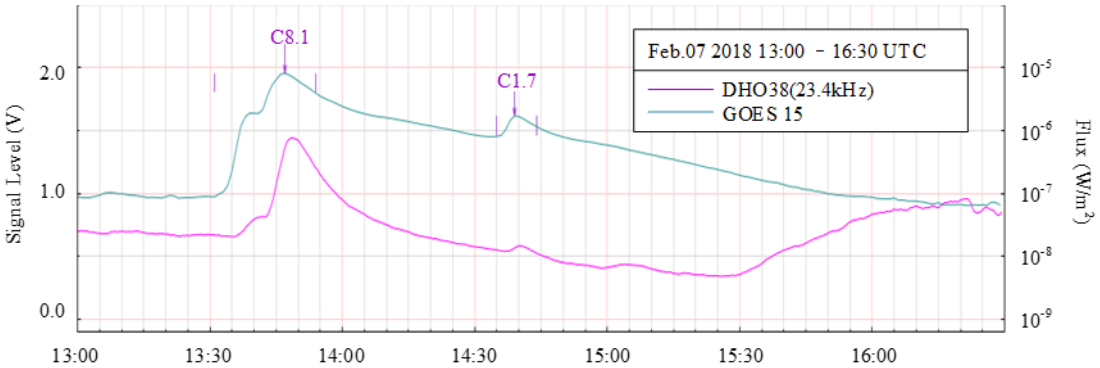

FIGURE 14. The impact of sudden ionosphere disturbances on signals on February 7, 2018 [116].

This article has been accepted for publication in a future issue of this journal, but has not been fully edited. Content may change prior to final publication. Citation information: DOI 10.1109/ACCESS.2019.2927811, IEEE Access

Except for communication disturbances, Ionospheric plasma charges the surface of the spacecraft as well. And hence the surface charging in LEO is bound to take space-charge effects, wake effects, and geomagnetic effects into account [117-119]. And hence detection and active control measures for spacecraft in LEO are generally referred to the simulation results of the charging potential and duration.

C. THE INNER RADIATION BELT

Since LEO is located at the bottom of the inner radiation belt, the radiation environment in high latitude and South Atlantic Anomaly is tougher than other areas in LEO [120-122], as shown in Figure 15. The disturbances of the geomagnetic field fluctuate the properties of high-energy particles intensely with the variation of time and locations. On the other hand, although protons predominate in high-energy particles in LEO, the solar proton event has less influence on the spacecraft there owing to the shielding by the geomagnetic field.

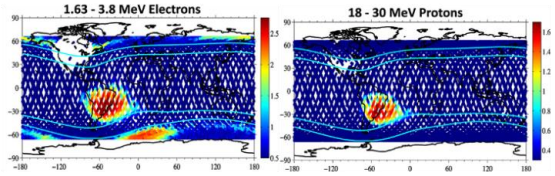

a) Energy map of high-energy particles at low and medium latitude.

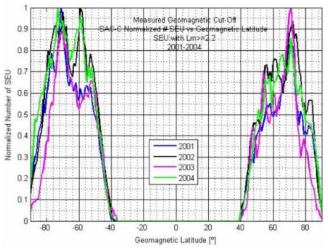

b) Statistical chart of the distribution of single event effects with latitude during 2001-2004.

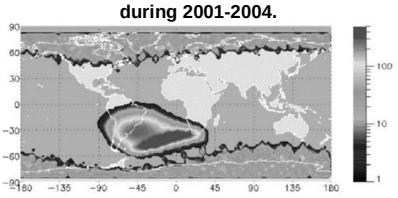

c) The flux of 10MeV proton during April - May 2001.

FIGURE 15. The map of high-energy particles in LEO [120-122].

However, the high-energy particles from solar activities could deposit in the polar regions along the magnetic lines of force. And therefore the radiation environment in polar regions is significantly affected by solar activities and the geomagnetic field. The intensity of high-energy protons there and the range of high-radiation area are positively correlated with the intensity of solar proton events and the severity of geomagnetic storms, respectively [123]. In conclusion, the radiation environment in polar areas in much harsher than that in low latitude.

In the radiation environment of LEO, the single event effects induced by high-energy protons are the most threatening to the spacecraft. For this reason, a series of models of protons in the inner radiation belt is established for calculation and analysis, in which PSB97 and LATRM are designed for LEO [124-125]. The flux spectrum of protons in a specific orbit could be obtained after the modification according to orbital parameters and the earth shielding effect.

D. MACROSCOPIC PARTICLE ENVIRONMENT IN LEO

The majority of the space debris is distributed in LEO, mainly concentrates in orbits with an altitude ranging from 450 km to 1200 km and an inclination ranging from 45 ° to 110 °[126]. And there are two density peaks at the altitude of 800 km and 1400 km, respectively [127], as outlined in Figure 16. High-inclination orbits experience denser space debris in all sizes, such as polar orbits and sun-synchronous orbits. Additionally, there is a flux peak of micrometeoroids nearby the altitude of 2500 km. It is reported that the flux of millimeter micrometeoroids and space debris close by the International Space Station is virtually equivalent [52]. Numerous spacecraft in LEO is threatened by high-density macroscopic particles every now and then.

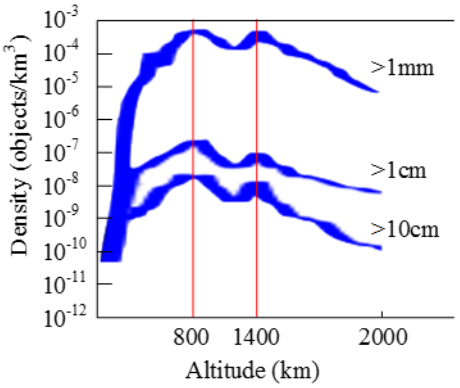

FIGURE 16. The map of high-energy particles in LEO [120-122].

Multiples of semi-empirical models have been proposed for macroscopic particle environment in LEO, like models used for space debris, such as SDPA, CHAIN, and ORDEM, as well as models used for micrometeoroids, such as Cours-Palais [128-130]. Coordinating radars based on ground and space are used for monitoring, at the service of warning and prevention by expert systems mentioned before. As for the spacecraft, they require capacity for deorbiting and capturing objects. As for the management, recycling, deorbiting, and burning down are both reasonable ways, where cleaning by a space-based laser has obvious potential in engineering application [131].

E. THE TEMPERATURE FIELD IN LEO

The spacecraft in LEO is heated by solar radiation, earth infrared and earth albedo, cooled by the cold black environment at the same time. Because of alternate heating and cooling periodically, the spacecraft experiences a large

This article has been accepted for publication in a future issue of this journal, but has not been fully edited. Content may change prior to final publication. Citation information: DOI 10.1109/ACCESS.2019.2927811, IEEE Access

temperature difference ranging from -101 ℃ to 93 ℃ [132], as exampled in Figure 17. Additionally, the spacecraft undergoes a dramatic gradient of temperature in the penumbra region. Since various materials are different with properties like thermal expansion coefficient, thermal deformation and vibration are inclined to happen to structures. And hence it is crucial to anticipate and control the changes of the temperature field [133].

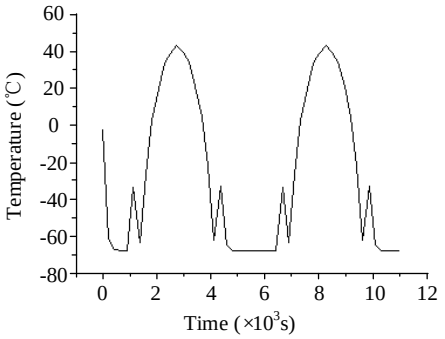

FIGURE 17. The temperature change of a feature point in an antenna in LEO [132].

IV. THE SPACE ENVIRONMENT IN M&H

M&H refers to a region above LEO, where MEO and HEO are separated by the GEO. With the development of satellite groups used for navigation and communication, M&H has occupied an increasingly important position. The space environment in M&H contains the plasma, radiation, macroscopic particle environment, and the temperature field, which are disturbed by geomagnetic field and solar activities to varying degrees.

A. MAGNETOSPHERIC PLASMA AND SOLAR WIND PLASMA

The plasma environment in M&H is mainly composited by magnetospheric plasma and solar wind plasma. Its particle energy spectrum is in a wide range and varies with regions [134], especially complicated in HEO. In addition to the background of cold plasma, hot plasma is frequently injected into M&H because of constant disturbance of geomagnetic storms and solar activities. As a consequence, the spacecraft in GEO could be charged to tens of thousands of volts every so often [135], as shown in Figure 18.

During the geomagnetic substorm, although the spacecraft in GEO has been severely charged in the shadow region, the charging is effectively suppressed by the photoelectron current in the sunshiny region [137]. The potential difference would be generated when the spacecraft is under different conditions at the same time. As the potential difference reaches the threshold, the electrostatic discharge would occur [138]. Additionally, the plasma also has a great impact on the transmission of signals for navigation satellites [139]. Seeing that the plasma environment in HEO is complex, the dual Maxwell distribution is applied to describe it in GEO [140]. Based on the law of surface charging obtained by algorithms like PIC, detection and active control measures of surface potential are developed [141].

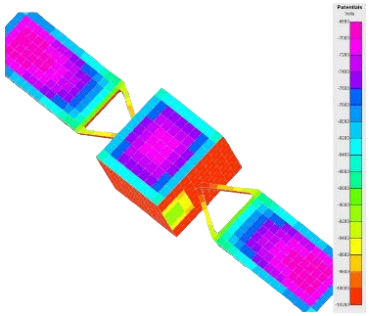

FIGURE 18. The result of stable surface charge of the spacecraft in GEO [136].

B. THE OUTER RADIATION BELT AND SOLAR PROTON EVENTS

The radiation environment in M&H mainly consists of electrons from the outer radiation belt and protons from solar proton events. A majority of navigation satellites, such as GPS and Beidou, are located at the center of the outer radiation belt, while the spacecraft in GEO is placed at the periphery of the outer radiation belt and experiences solar proton events occasionally. Moreover, the fluxes of electrons and protons near the altitude of 20000 km are both higher than that in GEO. Consequently, MEO has a more awful radiation environment than GEO during the solar minimum.

The flux of high-energy electrons in MEO varies with their intensity which is concerned with time. Seeing that the high-energy electron environment responses to geomagnetic storms nonlinearly, it is a dynamic system which changes violently [142]. The high-energy electron environment in MEO has different scales of quasi-periodic time-varying characteristics [143], while that in GEO has obvious fluctuations with local time every day and solar activities weekly [144]. The flux of high-energy electrons in GEO is negatively correlated with solar activities. During the solar minimum, its flux reaches the highest value around the spring equinox and the autumnal equinox, while it reaches the lowest value around the summer solstice and the winter solstice. It has different distributions during day and night. That is to say, it reaches the maximum at noon and the minimum at midnight in local time. Empirical models that are appropriate for M&H include AE-8, AE-9, FLUMIC, and PLOE [145-146]. Fitted and modified by logarithmic values [147], the nonlinear correlation between high-energy electrons and solar wind or geomagnetic Ap index could be resolved by methods like neural networks [148-149].

Since the energy and intensity of protons in the outer radiation belt are relatively low, the spacecraft orbiting higher than 24000 km is less affected by protons captured by the geomagnetic field. What they worry about more is protons derived from solar proton events. As the diminishment of the shielding effect of the geomagnetic field, the spacecraft operating in HEO suffers more severely than

This article has been accepted for publication in a future issue of this journal, but has not been fully edited. Content may change prior to final publication. Citation information: DOI 10.1109/ACCESS.2019.2927811, IEEE Access

those operating in MEO with the same inclination. Additionally, due to the sediment of particles in polar area, the spacecraft with high inclination is more likely to be impaired by solar proton events than those with smaller inclination. Models appropriate for high-energy protons in M&H contain AP-8, CRRES PRO, TPM-1, etc., in which AP-8, AP-9, and JPL are able to apply to GEO [150-151].

In M&H, the high-energy electrons are responsible for internal charging and total dose effects [152], while the high-energy protons are answerable for single event effects and displacement damage. According to the statistics in 2015 [153], the correlation between abnormalities of the flux of high-energy electrons and satellite anomalies was as high as 80%. Since internal charging acts as the main cause of anomalies in GEO [65], the high-energy electrons are the most threatening in the radiation environment of GEO.

Figure 19 shows the risk assessment of internal charging in different orbits given by NASA. The chart provides a quick idea about whether internal charging should be of concern in a simple way. In the meanwhile, the situations of a few common satellites are marked on it. As we can see, the internal charging is not the principal problem in LEO, while most of the spacecraft in M&H including GEO is at much higher risk. On the basis of empirical models, the internal electric field of the spacecraft can be simulated by taking advantages of software like DICTAT and SEAES [154-156].

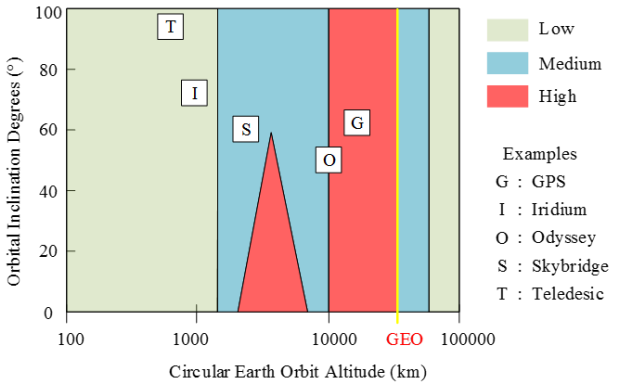

FIGURE 19. **The map of internal charging risk [157].**

C. MACROSCOPIC PARTICLE ENVIRONMENT IN M&H

The density of space debris in M&H is much less than that in LEO. Even if at the peaks of each size, it is still 1-2 orders of magnitude smaller, and the density of space debris reduced drastically in regions higher than GEO. Nevertheless, except for regions at the bottom of MEO, space debris in M&H cannot be cleared up by the atmosphere, which leads to a long lifespan and rapid increase of it. Figure 20 demonstrates that there are two density peaks around 20000 km and GEO [127]. Compared with LEO, low as the probability of collision is, space debris is still threatening for spacecraft operating around the peaks. On the other side, the flux of micrometeoroids in M&H is far from close to that in LEO, and therefore space debris the main hazard of macroscopic particle environment.

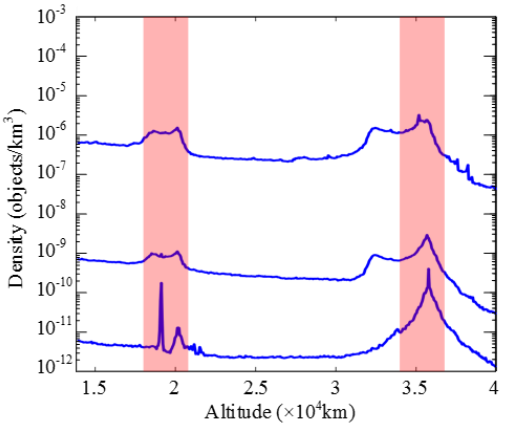

FIGURE 20. **The density of space debris in M&H [127].**

Ground-based radars have difficulties in monitoring dangerous debris in M&H accurately due to the high altitude. Whereupon, optical observation is the main approach with the guidance of efficient search strategies [158]. Multiples of semi-empirical models for M&H have been proposed, such as MASTER, LUCA, and SDM/STAT [128-130]. The spacecraft in M&H requires capacity for deorbiting and sending items to graveyards. Besides, capturing in-orbit should be available for space debris in specific orbit [159-161], to dispose of them by collecting or removing [70, 72].

D. THE TEMPERATURE FIELD IN M&H

Spacecraft in M&H suffers space external heat containing solar radiation, earth infrared, earth albedo, as well as the heat sink of cold black environment. Seeing that the effects of earth infrared and albedo are one order of magnitude smaller than that of solar radiation at least, the temperature changing could mainly consider the effects of solar radiation in some cases [162].

The temperature difference in M&H is larger than that in LEO, as exampled in Figure 21. The maximum difference of an antenna with an aperture of 7.5 m could be up to 200 ℃ at the same time [163]. Large difference like this is inclined to induce thermal deformation and vibration which is harmful to operation. However, since the spacecraft in M&H takes a longer time to pass through the penumbra region, it suffers a relatively small gradient of temperature than that in LEO.

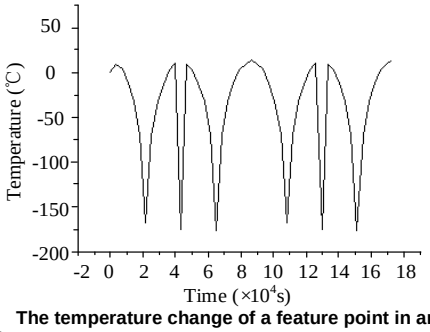

FIGURE 21. **The temperature change of a feature point in an antenna in GEO [132].**

V. CONCLUSIONS

There are distinct differences in all kinds of environmental components between LEO and M&H. The environmental components primarily considered for spacecraft in LEO contain the neutral atmosphere, ionospheric plasma, the inner radiation belt, macroscopic particle environment, the temperature field, and the geomagnetic field. Due to its low altitude, LEO is the main affected region of the upper atmosphere and the geomagnetic field, which are peculiar to LEO. The ionospheric plasma is predominant in the plasma environment in LEO, with low energy and high concentration. Most region of LEO is located at the bottom of the inner radiation belt, and South Atlantic Anomaly and polar areas are most severely affected by the radiation. Besides, macroscopic particles are densest in LEO, and threats for spacecraft with high inclination are larger than those with small inclination. Except for the large temperature difference, spacecraft in LEO suffers a great temperature gradient in the penumbra region. The polar orbit is a special type of orbits in LEO. Particles and plasma settle there and the charged particle environment is more horrible than low-latitude regions. Shielded by the geomagnetic field, LEO is less influenced by hot plasma and high-energy particles ejected by solar activities. On the other hand, due to the intense geomagnetic field, the neutral atmosphere, plasma, and radiation are sensitive to geomagnetic disturbances.

The environmental components primarily considered for spacecraft in M&H contain the plasma, radiation, macroscopic particle environment, and the temperature field. Due to weak protection of the geomagnetic field, the spacecraft in M&H is susceptible to solar activities. The plasma environment in M&H consists of magnetospheric plasma and solar wind plasma. With hot plasma injected in the background of cold plasma, the plasma environment in M&H has high energy but low concentration. Besides, the radiation environment is affected by both the Van Allen radiation belt and solar cosmic rays. During the solar minimum, the radiation in MEO is even worse than that in GEO. Additionally, sparse as macroscopic particles in M&H, the threats are serious than that in LEO, because of the limitation of macroscopic particle management conditions, HEO in particular. Moreover, compared with LEO, there is a larger temperature difference for spacecraft in M&H to suffer. However, the temperature gradient is little smaller owing to the relatively long time when passing through the penumbra area.

It can be seen that various space environmental components have different impacts on the spacecraft operation, which could lead to numerous anomalies. It is noticeable that the specific environment analysis for different orbits is the very demanding basis of spacecraft maintenance. This paper can provide technological support for the design of spacecraft in different orbits.

REFERENCES

[1] Liou J C, Rossi A, Krag H, et al. Stability of the future LEO environment[J]. Inter Agency Space Debris Coordination Committee. Working Group, 2013, 2.

[2] "Definitions of geocentric orbits from the Goddard Space Flight Center". User support guide: platforms. NASA Goddard Space Flight Center. Archived from the original on May 27, 2010. Retrieved 2012-07-08.

[3] UCS Satellite Database[EB/OL]. the Union of Concerned Scientists, 2019 [2019-5]. https://www.ucsusa.org/nuclear-weapons/space-weapons/satellite-database.

[4] Kaplan M, Hudaverdi M. The correlations of space weather and satellite anomalies: RASAT[C]// International Conference on Recent Advances in Space Technologies. IEEE, 2013.

[5] Koons H C, Mazur J E, Selesnick R S, et al. The Impact of the Space Environment on Space Systems[J]. Proc.spacecraft Charging Tech.conf, 2000, -1.

[6] Leach R D, Alexander M B. Spacecraft System Failures and Anomalies Attributed to the Natural Space Environment[J]. National Aeronautics & Space Administration Nasa Reference Publication, 1996.

[7] Hastings D, Garrett H. Spacecraft-environment interactions[M]. Cambridge university press, 2004.

[8] Banks B A, Miller S K R. Overview of Space Environment Effects on Materials and GRC's Test Capabilities[J]. 2006.

[9] Arnold G S, Peplinksi D R . Reaction of high-velocity atomic oxygen with carbon[J]. AIAA Journal, 1986, 24(4):673-677.

[10] De Groh K K, Banks B A, Mccarthy C E, et al. MISSE 2 PEACE polymers atomic oxygen erosion experiment on the international space station[J]. High Performance Polymers, 2008, 20(4-5): 388-409.

[11] Banks B A, de Groh K K, Backus J A. Atomic Oxygen Erosion Yield Predictive Tool for Spacecraft Polymers in Low Earth Orbit[J]. 2008.

[12] Banks B A, de Groh K K, Miller S K. Low earth orbital atomic oxygen interactions with spacecraft materials[J]. MRS Online Proceedings Library Archive, 2004, 851.

[13] Yiğit E. Atmospheric and Space Sciences: Ionospheres and Plasma Environments[M]. Springer, 2017.

[14] Bonin G, Orr N, Zee R, et al. Solar Array Arcing Mitigation for Polar Low-Earth Orbit Spacecraft[J]. 2010.

[15] Yang J, Su W, Mao G, et al. On Calculating Effectiveness of Plasma Defense against Low-Orbit Spy Satellite[J]. Journal of Northwestern Polytechnical University, 2005. (in Chinese).

[16] Mandell M J, Davis V A, Gardner B M, et al. NASCAP-2K: An Overview[J]. 2004.

[17] Comparison of Low Earth Orbit Wake Current Collection Simulations Using Nascap-2k, SPIS, and MUSCAT Computer Codes[J]. IEEE Transactions on Plasma Science, 2013, 41(12):3303-3309.

[18] Mateo-Velez J C , Jean-Fran ̧ois Roussel, Inguimbert V , et al. SPIS and MUSCAT Software Comparison on LEO-Like Environment[J]. IEEE Transactions on Plasma Science, 2012, 40(2):177-182.

[19] Forestl J, Eliasson L, Hilgers A. A new spacecraft plasma interactions simulation software, PicUp3D/SPIS[C]//7th Spacecraft charging conference, Noordwijk, the Netherlands. 2001, 5: 515-520.

[20] Birdsall C K, Langdon A B. Plasma physics via computer simulation[M]. CRC press, 2004.

[21] Torkar K, Nakamura R, Tajmar M, et al. Active spacecraft potential control investigation[J]. Space Science Reviews, 2016, 199(1-4): 515-544.

[22] Riedler W , Torkar K , F. R ̈UDENAUER, et al. ACTIVE SPACECRAFT POTENTIAL CONTROL[J]. Space Science Reviews, 1997, 79(1-2):271-302.

[23] Sen Z. Satellite On-board Failure Statistics and Analysis[J]. Spacecraft Engineering, 2010.

[24] Leung P, Scott J, Seki S, et al. Arcing on space solar arrays. 11th Spacecraft Charging Technology Conference, 2010.

[25] Goiffon V, Estribeau M, Marcelot O, et al. Radiation Effects in Pinned Photodiode CMOS Image Sensors: Pixel Performance Degradation Due to Total Ionizing Dose[J]. IEEE Transactions on Nuclear Science, 2013, 59(6):2878-2887.

[26] Miller F, Luu A, Prud'Homme F, et al. Characterization of Single-Event Burnout in Power MOSFET Using Backside Laser Testing[J]. IEEE Transactions on Nuclear Science, 2006, 53(6):3145-3152.
[27] Sawyer D M, Vette J I. AP-8 trapped proton environment for solar maximum and solar minimum[J]. Nasa Sti/recon Technical Report N, 1976, 77.
[28] Xapsos M A, Summers G P, Barth J L, et al. Probability model for cumulative solar proton event fluences[C]// 1999 Fifth European Conference on Radiation and Its Effects on Components and Systems. RADECS 99 (Cat. No.99TH8471). IEEE, 2002.
[29] Vette J I. The AE-8 trapped electron model environment[J]. Nasa Sti/recon Technical Report N, 1991, 92.
[30] Rodgers D J, Hunter K. The FLUMIC electron environment model[C]//8 th Spacecraft Charging Technology Conference. 2003.
[31] Tang H H K. SEMM-2: A new generation of single-event-effect modeling tools[J]. IBM Journal of Research & Development, 2008, 52(3):233-244.
[32] Weller R A, Mendenhall M H, Reed R A, et al. Monte Carlo simulation of single event effects[J]. IEEE Transactions on Nuclear Science, 2010, 57(4): 1726-1746.
[33] Raine M, Hubert G, Gaillardin M, et al. Monte Carlo prediction of heavy ion induced MBU sensitivity for SOI SRAMs using radial ionization profile[J]. IEEE Transactions on Nuclear Science, 2011, 58(6): 2607-2613.
[34] Wilson J W, Cucinotta F A, Kim M H, et al. Optimized shielding for space radiation protection[J]. Physica medica: PM: an international journal devoted to the applications of physics to medicine and biology: official journal of the Italian Association of Biomedical Physics (AIFB), 2001, 17 Suppl 1(1):67.
[35] Durante, Marco. Space radiation protection: Destination Mars[J]. Life Sciences in Space Research, 2014, 1:2-9.
[36] Yui C C, Swift G M, Carmichael C, et al. SEU mitigation testing of Xilinx Virtex II FPGAs[C]// Radiation Effects Data Workshop. 2003.
[37] Adams Jr J H, Hathaway D H, Grugel R N, et al. Revolutionary concepts of radiation shielding for human exploration of space[J]. 2005.
[38] Baker D N, Blake J B, Callis L B, et al. Relativistic electron acceleration and decay time scales in the inner and outer radiation belts: SAMPEX[J]. Geophysical Research Letters, 1994, 21(6).
[39] Baker D N, Kanekal S G, Li X, et al. An extreme distortion of the Van Allen belt arising from the 'Hallowe'en'solar storm in 2003[J]. Nature, 2004, 432(7019): 878.
[40] Goldstein, J. Dynamic relationship between the outer radiation belt and the plasmapause during March–May 2001[J]. Geophysical Research Letters, 2005, 32(15):L15104.
[41] ESA. Analysis and Prediction[EB/OL]. EAS's Space Debris Office, 2018[2019-5]. https://www.esa.int/Our_Activities/Operations/Space_Safety_Security/Space_Debris/Analysis_and_prediction.
[42] National Research Council. Orbital debris: A technical assessment[M]. National Academies Press, 1995
[43] Kearsley A T, Drolshagen G, Mcdonnell J A M, et al. Impacts on Hubble Space Telescope solar arrays: Discrimination between natural and man-made particles[J]. Advances in Space Research, 2005, 35(7):1254-1262.
[44] Christiansen E L . Design and performance equations for advanced meteoroid and debris shields[J]. Int.j.impact Engng, 1993, 14(1):145-156.
[45] Jenkin A B, Peterson G E. Collision risk management in geosynchronous orbit[J]. Advances in Space Research, 2004, 34(5): 1188-1192.
[46] Hyde J L, Christiansen E L, Kerr J H. Meteoroid and orbital debris risk mitigation in a low earth orbit satellite constellation[J]. International journal of impact engineering, 2001, 26(1-10): 345-356.
[47] Drolshagen G. Hypervelocity impact effects on spacecraft[C]//Meteoroids 2001 Conference. 2001, 495: 533-541.
[48] McNeil W J, Lai S T, Murad E. Charge Production due to Leonid Meteor Shower Impact on Spacecraft Surfaces[C]//6th Spacecraft Charging Technology. 1998: 187-191.
[49] Chobotov V A, Jenkin A B. Analysis of the micrometeoroid and debris hazard posed to an orbiting parabolic mirror[J]. Space Debris, 2000, 2(1): 9-40.
[50] Schonberg W P. Protecting spacecraft against meteoroid/orbital debris impact damage: an overview[J]. Space Debris, 1999, 1(3):195-210.
[51] Dittberner G J, Fudge M L, Huth J S, et al. Examining simplifying assumptions of probability of collisions in LEO[C]//Proceedings of the First European Conference on Space Debris, Darmstadt, Germany. 1993: 485-489.
[52] Ekstrand V, Drolshagen G. Comparison of meteoroid and space debris fluxes to spacecraft in Earth orbit[C]//Meteoroids 2001 Conference. 2001, 495: 543-550.
[53] Kessler D J. Space Station Program Natural Environment Define for Design Revision A [R]. NASA SSP-30425, 1991.
[54] Whittlesey A, Garrett H B, D. NASA's Technical Handbook for Avoiding On-Orbit ESD Anomalies Due to Internal Charging Effects[C]// Spacecraft Charging Technology. 6th Spacecraft Charging Technology, 1996.
[55] Mehrholz D, Leushacke L, Flury W, et al. Detecting, tracking and imaging space debris[J]. ESA Bulletin. Bulletin ASE. European Space Agency, 2002, 109(109):128-134.
[56] Schildknecht T. Optical surveys for space debris[J]. Astronomy & Astropysics Review, 2007, 14(1):41-111.
[57] Tommei G , Milani A , Rossi A . Orbit determination of space debris: admissible regions[J]. Celestial Mechanics and Dynamical Astronomy, 2007, 97(4):289-304.
[58] Jehn R . Comparison of the 1999 beam-park experiment results with space debris models[J]. Advances in Space Research, 2001, 28(9):1367-1375.
[59] Moorhead A V. Meteoroid environment modeling: the Meteoroid Engineering Model and shower forecasting[J]. 2017.
[60] Cour-Palais B G. NASA space vehicle design criteria-environment. Meteorid environment model-1969/near earth to lunar surface[J]. 1969.
[61] Staubach P, Grün E. Development of an upgraded meteoroid model[J]. Advances in Space Research, 1995, 16(11): 103-106.
[62] Frye J W. Collision probability estimate method for impact generated low earth orbit space debris clouds[C]//Astrodynamics 1991. 1992: 287-310.
[63] Chobotov V A, Mains D L. Tether satellite system collision study[J]. Acta Astronautica, 1999, 44(2):99-112.
[64] Christiansen E L, Nagy K, Hyde J. Bumper 3 Update for IADC Protection Manual[J]. 2016.
[65] Wang Haifu, Yu Qingbo, LiuYouying, et al. M/OD Risk Assessment System and Its Applications[J]. Journal of Beijing Institute of Technology, 2009, 18(1):6-10
[66] Schäfer F K, Herrwerth M, Hiermaier S J, et al. Shape effects in hypervelocity impact on semi-infinite metallic targets[J]. International Journal of Impact Engineering, 2001, 26(1-10): 699-711.
[67] Turner R J, Taylor E A, McDonnell J A M, et al. Cost effective honeycomb and multi-layer insulation debris shields for unmanned spacecraft[J]. International Journal of Impact Engineering, 2001, 26(1-10): 785-796
[68] Destefanis R, Schäfer F, Lambert M, et al. Enhanced space debris shields for manned spacecraft[J]. International Journal of Impact Engineering, 2003, 29(1-10): 215-226.
[69] Liou J C, Johnson N L. Risks in space from orbiting debris[J]. 2006.
[70] Bender M. Flexible and low-cost dragon spacecraft for orbital debris removal[C]// Proc. NASA/DARPA Orbital Debris Conference. 2009.
[71] Hoyt R. RUSTLER[C]//Architecture and technologies for lowcost remediation of the LEO large debris population", NASA/DARPA Orbital Debris Conference. 2009.
[72] Kawamoto S, Ohkawa Y. Strategies and technologies for cost effective removal of large sized objects[C]//Proc. NASA/DARPA Orbital Debris Conference. 2009.
[73] Bonnal C, Ruault J M, Desjean M C. Active debris removal: Recent progress and current trends[J]. Acta Astronautica, 2013, 85: 51-60.
[74] Wang Z, Wang B, Xu L, et al. Feedback-Added Pseudoinverse-Type Balanced Minimization Scheme for Kinematic Control of

Redundant Robot Manipulators[J]. IEEE Access, 2019, 7: 23806-23815.

[75] Chen X, Qin S. Kinematic modeling for a class of free-floating space robots[J]. IEEE Access, 2017, 5: 12389-12403.

[76] Vasile M, Maddock C, Saunders C. Orbital debris removal with solar concentrators[C]//61st International Astronautical Congress, IAC 2010. 2010: Paper IAC-10. A6. 4.

[77] Smith E S, Sedwick R J, Merk J F, et al. Assessing the potential of a laser-ablation-propelled tug to remove large space debris[J]. Journal of Spacecraft and Rockets, 2013, 50(6): 1268-1276.

[78] Phipps C R, Baker K L, Libby S B, et al. Removing orbital debris with lasers[J]. Advances in Space Research, 2012, 49(9): 1283-1300.

[79] Phipps C R. A laser-optical system to re-enter or lower low Earth orbit space debris[J]. Acta Astronautica, 2014, 93: 418-429.

[80] ESA. Space Debris by the Numbers[EB/OL]. Germany: EAS's Space Debris Office, 2019[2019-5]. https://www.esa.int/Our_Activities/Operations/Space_Safety_Security/Space_Debris/Space_debris_by_the_numbers

[81] Sharma J, Ratanpal B S, Pirzada U M, et al. Simulation of Motion of Satellite under the Effect of Oblateness of Earth and Atmospheric Drag[J]. 2016.

[82] Kono M, Roberts P H. Recent geodynamo simulations and observations of the geomagnetic field[J]. Reviews of Geophysics, 2002, 40(4): 4-1-4-53.

[83] Gonzalez W D, Joselyn J A, Kamide Y, et al. What is a geomagnetic storm?[J]. Journal of Geophysical Research, 1994, 99(A4):5771.

[84] Shue J H, Song P, Russell C T, et al. Magnetopause location under extreme solar wind conditions[J]. Journal of Geophysical Research: Space Physics, 1998, 103(A8): 17691-17700.

[85] Macmillan S, Quinn J M. The 2000 revision of the joint UK/US geomagnetic field models and an IGRF 2000 candidate model[J]. Earth, Planets and Space, 2000, 52(12):1149-1162.

[86] Kim C, Li Q, Kuo C C J. Fast intra-prediction model selection for H. 264 codec[C]//Multimedia Systems and Applications VI. International Society for Optics and Photonics, 2003, 5241: 99-111.

[87] Xiaodi W, Chaochao H, Yongshun L, et al. Surface temperature and infrared feature of a satellite[J]. infrared and laser engineering, 2011, 40(5): 805-810.

[88] Bhanderi D, Bak T. Modeling Earth albedo for satellites in Earth orbit[C]//AIAA Guidance, Navigation, and Control Conference and Exhibit. 2005: 6465.

[89] Zarda P R, Anderson T, Baum F. FEM/SINDA: Combining the strengths of NASTRAN, SINDA, I-DEAS, and PATRAN for thermal and structural analysis[J]. 1993.

[90] Liu C, Xie J, Wang Y, et al. Distributed State Estimation for Networked Spacecraft Thermal Experiments Over Sensor Networks With Randomly Varying Transmission Delays[J]. IEEE Access, 2018, 6: 56658-56665.

[91] Cotten S B. Design, Analysis, Implementation, and Testing of the Thermal Control, and Attitude Determination and Control Systems for the CanX-7 Nanosatellite Mission[D]. , 2014.

[92] Phoenix A A, Wilson E. Adaptive Thermal Conductivity Metamaterials: Enabling Active and Passive Thermal Control[J]. Journal of Thermal Science and Engineering Applications, 2018, 10(5): 051020.

[93] Liu J, Li Y, Wang J. Modeling and analysis of MEMS-based cooling system for nano-satellite active thermal control[C]//2008 2nd International Symposium on Systems and Control in Aerospace and Astronautics. IEEE, 2008: 1-6.

[94] BROWN R, CANNADAY S. Electron-ultraviolet radiation effects on thermal control coatings[C]//3rd Thermophysics Conference. 1968: 779.

[95] Koskinen H. Space Weather: From Solar Storms to the Technical Challenges of the Space Age[M]//From the Earth's Core to Outer Space. Springer, Berlin, Heidelberg, 2012: 265-278.

[96] Qu Z, Zhang G, Cao H, et al. LEO satellite constellation for internet of things[J]. IEEE Access, 2017, 5: 18391-18401.

[97] Reddy M R . Effect of low earth orbit atomic oxygen on spacecraft materials[J]. Journal of Materials Science, 1995, 30(2):281-307.

[98] Banks B A, Stueber T J, Norris M J . Monte Carlo Computational Modeling of the Energy Dependence of Atomic Oxygen Undercutting of Protected Polymers[M]// Protection of Space Materials from the Space Environment. Springer Netherlands, 2001

[99] Banks B A, Backus J A, Manno M V, et al. Prediction of Atomic Oxygen Erosion Yield for Spacecraft Polymers[J]. Journal of Spacecraft and Rockets, 2011, 48(1):14-22.

[100] Lee C H, Chen L W . Reactive Probability of Atomic Oxygen with Material Surfaces in Low Earth Orbit[J]. Journal of Spacecraft & Rockets, 1971, 37(37):252-256.

[101] Miyazaki E, Tagawa M, Yokota K, et al. Investigation into tolerance of polysiloxane-block-polyimide film against atomic oxygen. Acta Astronaut[J]. Acta Astronautica, 2010, 66(5):922-928.

[102] Banks B, Mirtich M, Rutledge S, et al. Ion beam sputter-deposited thin film coatings for protection of spacecraft polymers in low earth orbit[C]//23rd Aerospace Scie30nces Meeting. 1985: 420.

[103] Bedra L, Rutigliano M, Balat-PichelinM, et al. Atomic Oxygen Recombination on Quartz at High Temperature:? Experiments and Molecular Dynamics Simulation[J]. LANGMUIR, 2006, 22(17):7208-7216.

[104] Liu Y, Liu X, Li G, et al. Numerical investigation on atomic oxygen undercutting of the protective polymer film using Monte Carlo approach[J]. Applied Surface Science, 2010, 256(20):6096-6106.

[105] Jing A, Wei Z, Dongsheng Y. Atomic oxygen environment analysis technology for low earth orbit spacecraft[C]// Prognostics & System Health Management Conference. IEEE, 2017.

[106] De Groh K K, Banks B A, Mccarthy C E, et al. MISSE 2 PEACE polymers atomic oxygen erosion experiment on the international space station[J]. High Performance Polymers, 2008, 20(4-5): 388-409.

[107] Bank B A, de Groh K K, Backus J A. Atomic Oxygen Erosion Yield Predictive Tool for Spacecraft Polymers in Low Earth Orbit[J]. 2008.

[108] Banks B A, de Groh K K, Miller S K. Low earth orbital atomic oxygen interactions with spacecraft materials[J]. MRS Online Proceedings Library Archive, 2004, 851.

[109] Yigit E. Atmospheric and Space Sciences: Ionospheres and Plasma Environments[J]. Atmospheric and Space Sciences: Ionospheres and Plasma Environments, by E. Yigit. SpringerBriefs in Earth Sciences, Vol. 2, 2018, 2018, 2.

[110] Cussac T, Clair M A, Pascale Ultré-Guerard, et al. The Demeter microsatellite and ground segment[J]. Planetary & Space Science, 2006, 54(5):413-427.

[111] Bleier T. Impending earthquakes have been sending us warning signals and people are starting to listen[J]. IEEE Spectrum, 2005: 17-21.

[112] Gussenhoven M S, Hardy D A, Rich F, et al. High-level spacecraft charging in the low-altitude polar auroral environment[J]. Journal of Geophysical Research: Space Physics, 1985, 90(A11): 11009-11023.

[113] Davies K. Ionospheric radio[M]. IET, 1990.

[114] Yiğit E, Knížová P K, Georgieva K, et al. A review of vertical coupling in the Atmosphere–Ionosphere system: Effects of waves, sudden stratospheric warmings, space weather, and of solar activity[J]. Journal of Atmospheric and Solar-Terrestrial Physics, 2016, 141: 1-12.

[115] Jixiang C. Using new material to analyze the effect of ionospheric disturbance on short-wave communication[C]//2006 7th International Symposium on Antennas, Propagation & EM Theory. IEEE, 2006: 1-3.

[116] Lionel Loudet. SID Monitoring Station[DB/OL]. Creative Commons, 2018[2019-5]. https://sidstation.loudet.org/data-en.xhtml.

[117] Yanhou X. A Research on Effects of Geomagnetics and Wakes on Spacecraft Surface Charging[J]. Chinese Spaceence & Technology, 1999.

[118] Parker L W. Potential Barriers and Asymmetric Sheaths due to Differential Charging of Nonconducting Spacecraft[R]. PARKER (LEE W) INC CONCORD MASS, 1978.

[119] Garrett H B. The charging of spacecraft surfaces[J]. Reviews of Geophysics, 1981, 19(4): 577-616.

[120] Li X, Selesnick R S, Baker D N, et al. Upper limit on the inner radiation belt MeV electron intensity[J]. Journal of Geophysical Research: Space Physics, 2015, 120(2): 1215-1228.

[121] Boatella C, Hubert G, Ecoffet R, et al. ICARE on-board SAC-C: More than 8 years of SEU and MCU, analysis and prediction[J]. IEEE Transactions on Nuclear Science, 2010, 57(4): 2000-2009.

[122] Falguere D, Boscher D, Nuns T, et al. In-flight observations of the radiation environment and its effects on devices in the SAC-C polar orbit[J]. IEEE transactions on nuclear science, 2002, 49(6): 2782-2787.

[123] Voss H D, Smith L G. Global zones of energetic particle precipitation[J]. Journal of Atmospheric and Terrestrial Physics, 1980, 42(3): 227-239.

[124] Huston S L, Pfitzer K A. Space environment effects: Low-altitude trapped proton model[J]. NASA Contract. Rep. NASA/CR, 1998, 208593.

[125] Gussenhoven M S , Mullen E G , Brautigam D H . Near-earth radiation model deficiencies as seen on CRRES[J]. Advances in Space Research, 1994, 14(10):927-941.

[126] Graham G A, Kearsley A T, Grady M M, et al. Hypervelocity impacts in low Earth orbit: Cosmic dust versus space debris[J]. Advances in Space Research, 1999, 23(1): 95-100.

[127] Rossi, Alessandro. Population models of space debris[J]. Proceedings of the International Astronomical Union, 2004, 2004(IAUC197):427-438.

[128] Rossi A, Anselmo L, Cordelli A, et al. Modelling the evolution of the space debris population[J]. Planetary and Space Science, 1998, 46(11-12):1583-1596.

[129] Johnson N, Christiansen E, Reynolds R, et al. NASA/JSC orbital debris models[C]//Second European Conference on Space Debris. 1997, 393: 225.

[130] Oswald M, Stabroth S, Wiedemann C. Final Report, Upgrade of the Master Model[J]. Institute of Aerospace Systems, Technische Universitat Braunschweig, European Space Agency, Document ID M, 2006, 5.

[131] Phipps C R. L′ ADROIT–A spaceborne ultraviolet laser system for space debris clearing[J]. Acta Astronautica, 2014, 104(1): 243-255.

[132] Cheng X X. Thermal Analysis Of Space Inflatable Deployment Sclerosis Film Antenna Structures[D]. Shanghai Jiao Tong University, 2011.(in Chinese).

[133] Storz M F, Bowman B R, Branson M J I, et al. High accuracy satellite drag model (HASDM)[J]. Advances in Space Research, 2005, 36(12): 2497-2505.

[134] Johnston W R, Lindstrom C D, Ginet G P. Characterization of radiation belt electron energy spectra from CRRES observations[C]// Agu Fall Meeting. AGU Fall Meeting Abstracts, 2010.

[135] Olsen R C. Record charging events from applied technology satellite 6[J]. Journal of Spacecraft and Rockets, 1987, 24(4): 362-366.

[136] Mandell M J, Davis V A, Cooke D L, et al. Nascap-2k Spacecraft Charging Code Overview[J]. IEEE Transactions on Plasma Science, 2006, 34(5):2084-2093.

[137] Mandell M J, Davis V A, Gardner B M, et al. NASCAP-2K: An Overview[J]. 2004.

[138] Lai S T, Tautz M F . Aspects of Spacecraft Charging in Sunlight[J]. IEEE Transactions on Plasma Science, 2006, 34(5):2053-2061.

[139] Frankel D S, Nebolsine P E, Miller M G, et al. Re-entry plasma induced pseudorange and attenuation effects in a GPS simulator[C]//Modeling, Simulation, and Calibration of Space-based Systems. International Society for Optics and Photonics, 2004, 5420: 65-75.

[140] Sjogren A , Eriksson A I , Cully C M . Simulation of Potential Measurements Around a Photoemitting Spacecraft in a Flowing Plasma[J]. IEEE Transactions on Plasma Science, 2012, 40(4):1257-1261.

[141] Patterson M J, Verhey T R, Soulas G, et al. Space Station Cathode Design, Performance, and Operating Specifications[J]. 1998.

[142] Reeves G D, Baker D N, Belgian R D, et al. The global response of relativistic radiation belt electrons to the January 1997 magnetic cloud[J]. Geophysical Research Letters, 1998, 25(17):3265–3268.

[143] Obara T, Matsumoto H, Koga K, et al. MDS-1 Observations of Highly Energetic Electron Environment in the Inner Magnetosphere[J]. Transactions of the Japan Society for Aeronautical & Space Sciences Space Technology Japan, 2009, 7(ists26):9030–9036.

[144] Love D P, Toomb D S, Wilkinson D C, et al. Penetrating electron fluctuations associated with GEO spacecraft anomalies[J]. IEEE Transactions on Plasma Science, 2000, 28(6):2075-2084.

[145] Choi H S, Lee J, Cho K S, et al. Analysis of GEO spacecraft anomalies: Space weather relationships[J]. Space Weather, 2011, 9(6).

[146] Boscher D M, Bourdarie S A, Friedel R H W, et al. Model for the geostationary electron environment: pole[J]. IEEE Transactions on Nuclear Science, 2003, 50(6):2278-2283.

[147] Li X, Baker D N, Teremin M, et al. Rapid enchancements of relativistic electrons deep in the magnetosphere during the May 15, 1997, magnetic storm[J]. Journal of Geophysical Research: Space Physics, 1999, 104(A3): 4467-4476.

[148] Fukata M, Taguchi S, Okuzawa T, et al. Neural network prediction of relativistic electrons at geosynchronous orbit during the storm recovery phase: effects of recurring substorms[C]//Annales Geophysicae. 2002, 20(7): 947-951.

[149] Ling A G, Ginet G P, Hilmer R V, et al. A neural network-based geosynchronous relativistic electron flux forecasting model[J]. Space Weather, 2010, 8(9): 1-14.

[150] Heynderickx D, Kruglanski M, Pierrard V. Trapped radiation environment model development[J]. 1998.

[151] Huston S L . Space Environments and Effects: Trapped Proton Model[J]. Nasa Sti/recon Technical Report N, 2002, 2.

[152] Whittlesey A, Garrett H. Avoiding problems caused by spacecraft on-orbit internal charging effects[J]. NASA Technical Handbook, 1999.

[153] Space Environment Prediction Center. Space environment situation forecast in June 2017 [EB/OL]. 2016[2019-5]. http://blog.sepc.ac.cn/?p=7456&cat=11. (in Chinese).

[154] Miyake H, Honjoh M, Maruta S, et al. Space charge accumulation in polymeric materials for spacecraft irradiated electron and proton[C]// Conference on Electrical Insulation & Dielectric Phenomena. 2007.

[155] Rodgers D J, Ryden K A, Wrenn G L, et al. Fitting of material parameters for DICTAT internal dielectric charging simulations using DICFIT[J]. Proceedings of International Symposium on Materials in A Space Environment, 2003, 540:609 - 613.

[156] O'Brien T P. SEAES-GEO: A spacecraft environmental anomalies expert system for geosynchronous orbit[J]. Space Weather-the International Journal of Research & Applications, 2009, 7(9).

[157] Whittlesey A, Garrett H B, D. NASA's Technical Handbook for Avoiding On-Orbit ESD Anomalies Due to Internal Charging Effects[C]// Spacecraft Charging Technology. 6th Spacecraft Charging Technology, 1996.

[158] Oswald M, Krag H, Wegener P, et al. Concept for an orbital telescope observing the debris environment in GEO[J]. Advances in Space Research, 2004, 34(5): 1155-1159.

[159] Aslanov V S, Yudintsev V V. The motion of tethered tug–debris system with fuel residuals[J]. Advances in Space Research, 2015, 56(7): 1493-1501.

[160] Liu H T, Zhang Q B, Yang L P, et al. Dynamics of tether-tugging reorbiting with net capture[J]. Science China Technological Sciences, 2014, 57(12): 2407-2417.

[161] Liu J, Cui N, Shen F, et al. Dynamics of Robotic Geostationary orbit Restorer system during deorbiting[J]. IEEE Aerospace and Electronic Systems Magazine, 2014, 29(11): 36-42.

[162] Gilmore D G, Bello M. Satellite thermal control handbook[M]. EI Segundo, CA: Aerospace Corporation Press, 1994.

[163] Farmer J T, Wahls D M, Wright R L, et al. Thermal distortion analysis of an antenna-support truss in geosynchronous orbit[J]. Journal of Spacecraft and Rockets, 1992, 29(3):386-393.

YIFAN LU was born in Harbin, Heilongjiang Province in 1989. He received the B.S. and Ph.D. degrees in mechanical engineering from the Harbin Institute of Technology in 2012 and 2018. He is currently an assistant professor in Research Center of Aerospace Mechanism and Control and the State Key Laboratory of Robotics and System in Harbin Institute of Technology. His area of expertise is sensing and control of smart materials and structures. His main research interests include dynamic control of space membrane structures, precision control of shape memory alloy actuators, and novel lunar dust mitigation methods.

Qi Shao was born in Weihai, Shandong province, China in 1996. She received the B.S. degrees in machine design and manufacture and automation from the Harbin Institute of Technology, China, in 2018. She is currently pursuing the Ph.D. degree in aerospace science and technology at Harbin Institute of Technology, Harbin, China. She is mainly engaged in the research of active shape control of space membrane structures. Her research interests include dynamics of in-orbit gossamer spacecraft and spacecraft-environment interactions.

HONGHAO YUE, born in 1978, is currently a professor and PhD candidate supervisor in Research Center of Aerospace Mechanism Control, Harbin Institute of Technology, China. His main research interests include mechatronics engineering and active vibration control of smart structures. He has won 1 awards such as two national technological invention, 2 first prize of Heilongjiang's technological invention, and 1 two awards of science and technology progress of the whole army. More than 40 academic papers have been published in international famous periodicals and important international academic conferences, 1 English publications have been published, and 4 national invention patents have been obtained.

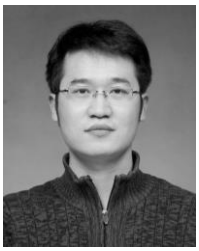

FEI YANG was born in yuncheng, Shanxi Province in 1985. He received the B.S. degrees in mechanical design and theory from the Guizhou University, Guiyang, in 2007 and the M.S. and Ph.D. degree in mechanical design and theory from Harbin Institute of Technology, Harbin, China in 2014.From 2014 to 2017, he was a Research Assistant with the Harbin Institute of Technology, Harbin, China. He is mainly involved in research on wheeled planetary vehicle mobility and space capture. He was promoted to associate professor in 2017.